Geophysical Research Letters®

Key Points:

- Convective motions can cause measurable ΔZ changes in time intervals as short as 30 s
- The reflectivity time-lapse rate technique relates to spatially and temporally coherent structures and the underlying convective motions
- The Investigations of Convective Updrafts mission radar sampling characteristics are adequate for capturing most of the ΔZ changes caused by convective motions

Correspondence to:

B. Dolan,
bdolan@atmos.colostate.edu

Time Resolved Reflectivity Measurements of Convective Clouds

Brenda Dolan[1] , **Pavlos Kollias[2,3]** , **Susan C. van den Heever[1]** , **Kristen L. Rasmussen[1]**,
Mariko Oue[2] , **Edward Luke[3]** , **Katia Lamer[3]** , **Bernat P. Treserras[4]**, **Ziad Haddad[5]** ,
Graeme Stephens[5] , **and V. Chandrasekar[1]**

[1]Colorado State University, Fort Collins, CO, USA, [2]School of Marine and Atmospheric Sciences, Stony Brook University, Stony Brook, NY, USA, [3]Brookhaven National Laboratory, Upton, NY, USA, [4]McGill University, Montreal, QC, Canada, [5]Jet Propulsion Laboratory, California Institute of Technology, Pasadena, CA, USA

Abstract National Aeronautics and Space Administration's Investigations of Convective Updrafts (INCUS) mission aims to document convective mass flux through changes in the radar reflectivity (ΔZ) in convective cores captured by a constellation of three Ka-band radars sampling the same convective cells over intervals of 30, 90, and 120 s. Here, high spatiotemporal resolution observations of convective cores from surface-based radars that use agile sampling techniques are used to evaluate aspects of the INCUS measurement approach using real observations. Analysis of several convective cells confirms that large coherent ΔZ structure with measurable signal (>5 dB) can occur in less than 30 s and are correlated with underlying convective motions. The analysis indicates that the INCUS mission radar footprint and along track sampling are adequate to capture most of the desirable ΔZ signals. This unique demonstration of reflectivity time-lapse provides the framework for estimating convective mass flux independent from Doppler techniques with future radar observations.

Plain Language Summary The vertical transport of water between Earth's surface and the upper troposphere afforded by convective storms is a driving factor of weather and climate. However, observing dynamic processes at the scales of convection has been a challenge due to the transient and rapidly evolving nature of convection, as well as sensor and resource limitations. High-resolution time-lapses of radar reflectivity are used to investigate the movement of air and water within deep, intense storms. This is a unique approach to understanding how water and air move throughout the atmosphere in strong storms. It is shown that large changes in reflectivity are apparent even over time scales less than 30 s, which are inferred to be due to strong vertical motions. A new National Aeronautics and Space Administration satellite mission called Investigations of Convective Updrafts seeks to use the same methods to estimate the movement of air and water globally across the tropics.

1. Introduction

Convective clouds play a critical role in the Earth's climate system, acting as sinks of total water in the atmospheric column through precipitation, thereby contributing to the atmospheric energy balance and water cycle. They also serve as a primary mechanism for the transport of thermal energy, moisture, and momentum through the troposphere, thereby significantly impacting the large-scale atmospheric circulation and local environment, and affecting the probability of subsequent cloud formation (e.g., Hartmann et al., 1984; Sherwood et al., 2014; Su et al., 2014). Because convective clouds evolve rapidly, their microphysical and kinematic properties and lifecycles are challenging to resolve in models, and even in observations (e.g., Fridlind et al., 2017; Marinescu et al., 2020; Oue et al., 2019). Noticeably, a knowledge gap on the convective updraft core properties (i.e., intensity, size, depth, lifecycle) and their dependency on environmental factors exists. Such measurements are not only particularly challenging to obtain over the remote tropical oceans, but also over land due to the transient and rapidly evolving nature of convection, as well as due to limitations of existing observing systems (e.g., Oue et al., 2019).

To methodically advance observation-based understanding of fundamental convective cloud processes, new observational approaches are needed. Emerging new technologies such as rapid scanning or phased-array radars can sample the rapid transient nature of convection (Bluestein et al., 2010; Kollias, Palmer, et al., 2022; Palmer et al., 2022; Tanamachi & Heinselman, 2016, etc.), but robust and detailed measurements of the vertical evolution

of convection have not been largely explored. In addition, the explosive growth of CubeSats (Peral et al., 2019; Stephens, Freeman, et al., 2020) and new planned satellite missions that all feature Doppler velocity measurements have the potential to provide the first global climatology of convective dynamics. For example, the joint European Space Agency and Japanese Aerospace Exploration Agency Earth Clouds, Aerosols, Radiation Explorer (EarthCARE) mission (Illingworth, et al., 2015; Wehr et al., 2023) will send the first W-band Doppler cloud profiling radar into space in 2024. In addition, National Aeronautics and Space Administration (NASA)'s Atmospheric Observing System mission is anticipated to include Doppler radar systems.

Of particular interest here is the NASA Earth Venture Mission Investigations of Convective Updrafts (INCUS) that encompasses three narrow-swath Ka-band profiling radar satellites, separated by 30, 90, and 120 s between the first and second, second and third, and first and third satellites, respectively. The INCUS radars will provide three curtain (along track and vertical) views of the radar reflectivity field of the same convective cells (Stephens, van den Heeven, et al., 2020; van den Heever, 2021). The INCUS convective mass flux (CMF) measurements are not based on the Doppler principle, but instead on time lapse measurements of reflectivity over very short times (termed "the Δt approach") to sample the mass flux on a global scale across the tropics. In contrast to Doppler measurements, estimating CMF from changes in reflectivity minimizes the sensitivity to the particle fall speeds. The INCUS CMF approach is based on the idea that over 30, 90, and 120 s time scales, convective dynamics can have a measurable impact on the convective core radar reflectivity structure. In this case, the time resolved radar reflectivity measurements can be used to retrieve the CMF.

Here, for the first time, the conceptual feasibility of Δt approach is investigated using real observations from high spatiotemporal vertical radar cross-section of convective cores acquired using the Multisensor Agile Adaptive Sampling (MAAS, Kollias et al., 2020) framework. MAAS utilizes a comprehensive data set in real time to guide ground-based sensors (radars) to track and sample convective cores (Lamer et al., 2023). Several convective cases of C-band radar data collected recently with the MAAS framework are examined to evaluate the Δt framework and demonstrate that coherent radar reflectivity changes can be related to underlying convective vertical air motion.

2. Methodology

A succession of Cloud, Precipitation, Aerosol, and Air Quality Field Experiments in the Coastal Urban Environment of Houston TX took place in the summer of 2022 (Jensen et al., 2022). In particular, the US Department of Energy (DOE) Atmospheric Radiation Measurement (ARM) Tracking Aerosol Convection interactions Experiment (TRACER) and the National Science Foundation (NSF) Experiment of Sea Breeze Convection, Aerosols, Precipitation, and Environment (ESCAPE) field campaigns targeted the study of isolated convective cells in the area of Houston, TX using novel radar cell tracking techniques. Documentation of the lifecycle of isolated convective cells with high spatiotemporal resolution was one key measurement requirement for both campaigns. To address this measurement need, the field campaigns employed the MAAS framework (Kollias et al., 2020; Lamer et al., 2023). MAAS used observations from the ground-based National Weather Service Next Generation Weather Radar (NEXRAD) in the Houston-Galveston area (KHGX, Crum et al., 1998), supplemented by observations from the Geostationary Operational Environmental Satellites (GOES-16) Geostationary Lightning Mapper, and the Advanced Baseline Imager (Griffith et al., 2017) to provide a real-time description (4D data cubes) of the atmospheric state around Houston. These "global" observations were used to identify and nowcast the future location of all convective cells in the Houston area. Using a set of rules, MAAS selected a particular convective cell for tracking and transmitted its current and future coordinates to both the second generation C-band Scanning ARM Precipitation Radar (CSAPR2, Kollias et al., 2020) and the CSU C-band Hydrological Instrument for Volumetric Observation (CHIVO). The CSAPR2 sampling strategy was based on sequences of Plan Position Indicator (PPI, constant elevation) sector scans that cover the horizontal extent of convective cells and Range Height Indicator (RHI, constant azimuth) scans that sampled the convective cells from the surface to their cloud top with high spatial resolution. The CSAPR2 RHIs were repeated approximately every 20 s. The CHIVO sampling strategy included only RHI scans with even higher temporal resolution (10 s). Both radars were sampling the same convective cells from different azimuth angles. The width of the CSAPR2 PPI sector scans and the azimuth of the CSAPR2 and CHIVO RHI scans were based on edge computing of key radar parameters such as the azimuth of the maximum reflectivity, the location of the maximum Vertically Integrated Liquid, maximum low-level convergence, and lightning strikes (Lamer et al., 2023). A detailed description of the MAAS
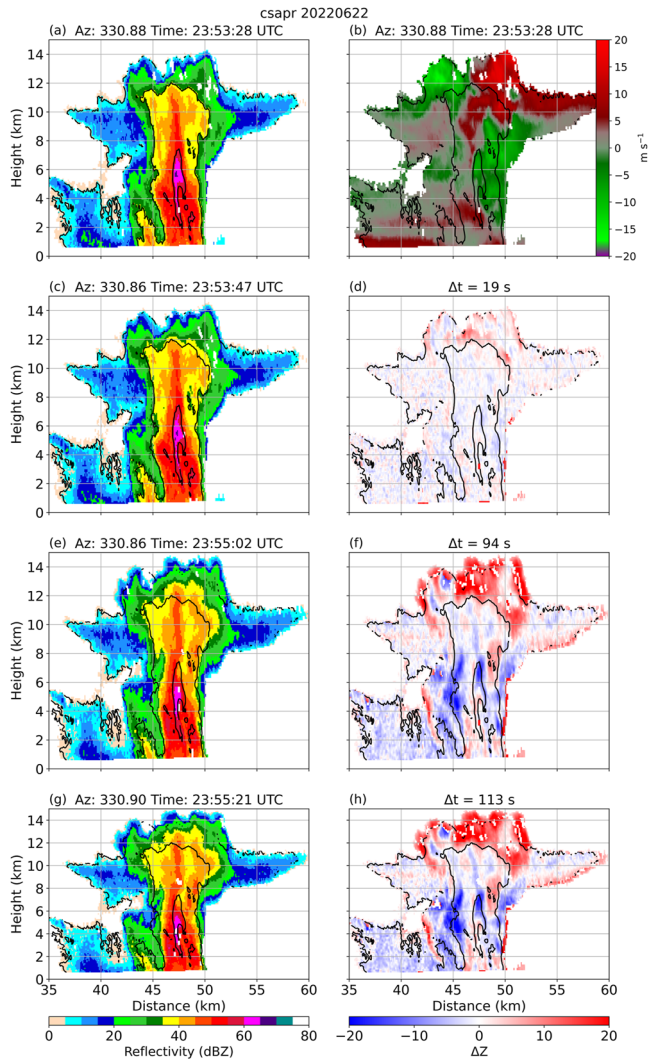
Figure 1. CSAPR2 RHIS at an azimuth of ~330° on 22 June 2022 at 23:53:28 UTC, and Δt = 19, 94, and 113 s. Black contours represent the 5-, 35-, and 55-dBZ contours at 23:53:28. (b) Radial velocity at t_0.

implementation in the context of the TRACER and ESCAPE field campaigns can be found in Lamer et al. (2023).

Here, sequences of RHI scans collected by either CSAPR2 or CHIVO along the same azimuth ($\pm 0.03°$) within 120 s of each other are selected to capture the vertical structure of convective cores as depicted by the radar reflectivity (Z) and its temporal evolution. Each RHI is gridded using the Lidar Radar Open Software Environment (LROSE, Bell et al., 2022) Radx2Grid with a grid rotation angle equal to the azimuth of the RHI, essentially reducing the data to a 2-dimensional grid of height and distance from the radar. Storm motion and advection are not specifically accounted for but are both small for the cases presented. In the selected cases, the horizontal environmental winds were weak throughout the column, with less than 3.5 m s^{-1} cross-RHI components, and generally less than 5 m s^{-1} along track. Thus, at the short time scales being considered here, the horizontal advective components are small. To capture the high-resolution aspects of the RHIs, the data were gridded to 100 m in the horizontal (x) and vertical (z) dimension (above ground level [AGL]).

Using the gridded radar observations, the change in radar reflectivity, herein called ΔZ, is calculated at each grid point by subtracting the reflectivity in dB scale ($\Delta Z = Z_e - Z_i$) between two different radar reflectivity frames collected at two different times ($\Delta t_s = t_e - t_i$), where the subscript i denotes the initial time, e denotes the time of the second RHI, and s is the elapsed time difference between the two radar frames in seconds. In the case where Z_i is missing, the ΔZ at that point is set to Z_e. A first example of radar observations at INCUS-like time intervals is depicted in Figure 1 and is generated using a sequence of four CSAPR2 RHI with Δt_e increments of e = 19, 94, and 113 s relative to the first RHI. This is the Δt approach that will be utilized by INCUS (van den Heever, 2021).

3. Results

3.1. Case 1: Assessment of Convective Storm Evolution From an Intense Deep Convective Core

The first case study is a convective core targeted by MAAS with the CSAPR2 radar at 23:53:28 UTC on 22 June 2022 (Figure 1). It is an isolated deep convective cell, fairly representative of the types of afternoon convection often observed in the diurnal cycle in the Houston area (Lamer et al., 2023; Oue et al., 2022). The well-developed convective cells exhibit a maximum radar reflectivity of more than 65 dBZ and echo top heights that reach 15 km (Figure 1). In addition to the series of CSAPR2 RHIs that provide high spatiotemporal resolution view of the convective core vertical structure, two consecutive CSAPR2 PPIs at 3° elevation at 23:53:17 and 23:54:52 UTC (Δt_{95}) are used to provide the horizontal extent of this isolated convective core (Figure 2). Despite its intensity and vertical extent, the convective core was less than 10 km wide (Figure 2). Although some increases in reflectivity at 3.0° elevation are noted over the 95 s (Figure 2), the overall storm complex has not advected horizontally during the span of the RHIs conducted (Figure 1).

At t_0 = 23:53:28 UTC (Figure 1a), the C-band radar reflectivity in the convective core exceeded 60 dBZ at around 6 km AGL, and the 35 dBZ (0 dBZ) echo top height was 12 km (14.2 km). At Δt_{19}, the ΔZ field indicates an increase in radar reflectivity above 10 km height on the order of +5 dB (0.3 dB s^{-1}), while the rest of the echo changes were very close to 0 dB (Figures 1c and 1d). The 35 dBZ (0 dBZ) echo top height increased by 100 m (300 m) to 12.1 km (14.5 km). While these changes in reflectivity and height are relatively small, they highlight the rapid evolution of convection through changes in reflectivity at very short time scales (19 s), even in non-severe deep convection. A plausible explanation for the increase in the radar reflectivity in the upper part of the convective cell is the lofting of condensate mass through the column by an underlying updraft. The radial
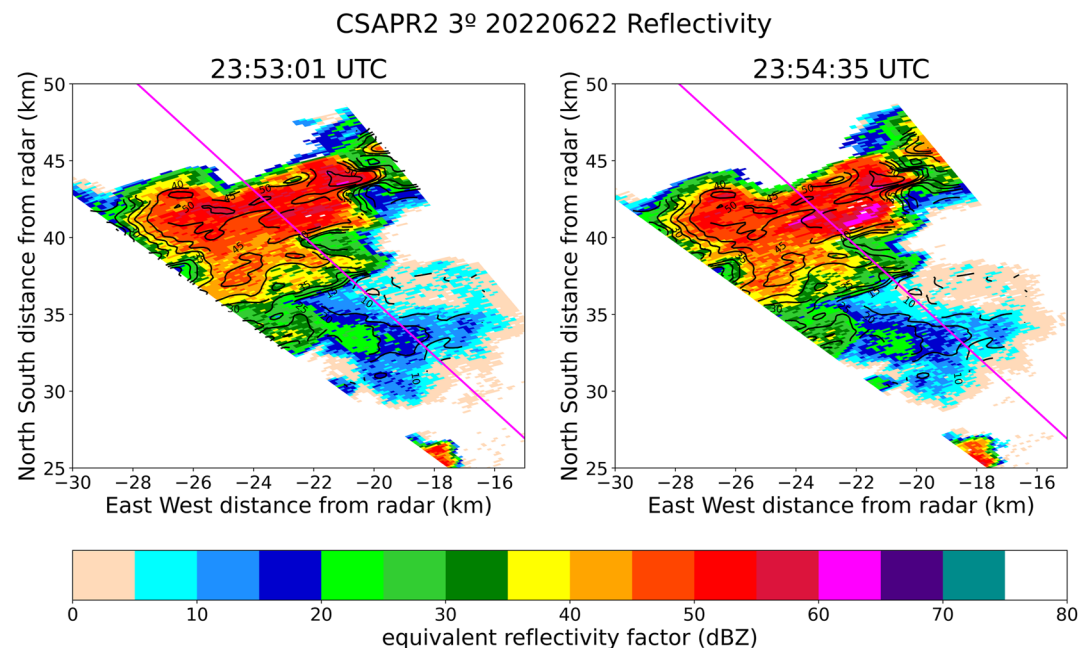
Figure 2. CSAPR2 consecutive Plan Position Indicator sectors (spaced by ~90 s) of Case 1 at 3° in elevation at 23:53:01 (left) and 23:54:35 UTC (right). The black contours are the reflectivity from the initial time (23:53:01 UTC) at 5 dB increments. The magenta line corresponds to the CSAPR RHIs shown in Figure 1.

Doppler velocity (Figure 1b) confirms the presence of an updraft (positive away radial winds at the upper part of the cloud) within the 35 dBZ area. The flow divergence and convective mass detrainment at the upper part of convective cell is nicely depicted by the opposite sign radial Doppler velocity values. It is also plausible that the updraft vertical extent reaches lower in the convective cell; however, the strongest changes in ΔZ are easier to detect near the upper part of the cloud suggesting that the relationship between updraft strength and ΔZ depends also on the background signal (Z_i).

More significant ΔZ changes throughout the storm are noted 94 s later by the time of the third RHI at Δt_{94} (Figures 1e and 1f). Reflectivity changes in the core aloft (>10 km) are up to +20 dB (0.2 dB s^{-1}), and the 35 dBZ (0 dBZ) echo top height has risen to 13 km (14.8 km), corresponding to a change of 1,000 m over 94 s, or an ascent rate of 10.6 m s^{-1}. On the other hand, ΔZ in the mid-levels (4–6 km) are dominated by negative changes in reflectivity on the order of −10 dB. Considering the rapid negative change in Z, we speculate that this could be related to precipitation fall out of hail and rain or size sorting, or contributions from horizontal advection. Further studies supported by LES-scale (100 m) model simulations will be required to better understand these processes and their relation to $\Delta Z/\Delta t$. Similarly, almost 2 min later (Δt_{113}, Figures 1g and 1h), the increases in reflectivity aloft are >20 dB, and decreases in the mid-levels exceed −20 dB. At lower levels (<4 km), small decreases in reflectivity are noted in the leading edge of the storm, whereas small positive changes on the order of 3 dB are evident in the core (Figures 1g and 1h). In general, reflectivity changes in the anvil are small (<|5| dB), although the largest changes are on the underside of the anvils which could be indicative of the anvil spreading out as well as stratiform fallout.

3.2. Case 2: The Effect of Temporal Resolution on Assessing Convective Storm Evolution

The higher temporal resolution of the CHIVO radar is used here to investigate time resolved radar reflectivity changes at even finer temporal resolutions than those proposed for the INCUS mission. On 16 September 2022 at 11:44:24 UTC, MAAS targeted a convective cell at 45 km at an azimuth of 132.63° from CHIVO. Case 2 features a much weaker convective core than Case 1, with a maximum reflectivity of 54 and 35 dBZ (0 dBZ) echo top height at t_0 of 10.4 km (13.5 km, Figure 3a). Local soundings (not shown) indicated significantly dry conditions in the mid-levels that could be responsible for the weaker convective conditions. As in Case 1, the Case 2 isolated convective core is narrow, spanning less than 10 km in the horizontal (not shown). At Δt_{17},
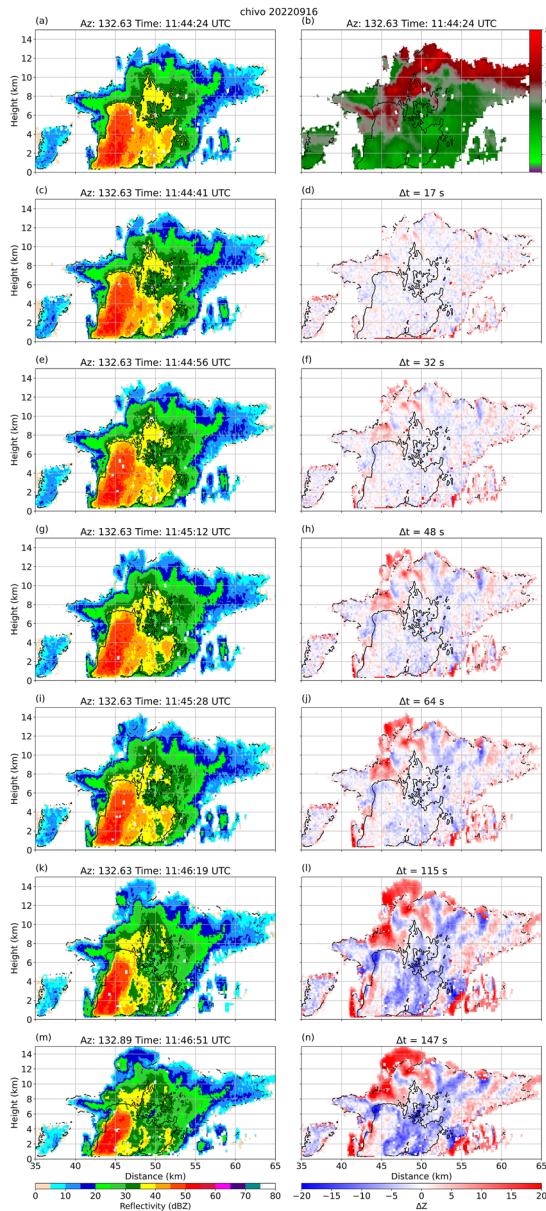
Figure 3. Timeseries of RHIs from the CHIVO radar on 16 September 2022 beginning at 11:44:24 UTC along the azimuth 123.6°. Reflectivity is shown at each time in the left panels, and reflectivity differences from t_0 (a) are in the right panels. (b) Radial velocity at t_0.

and similarly at Δt_{32}, changes in reflectivity are small ($<\pm5$ dB) throughout the echo depth (Figures 3c and 3d, 0.3 dB s^{-1}). However, some larger positive changes become apparent by Δt_{32} above the intense core at 45 km range and at 8 km AGL (Figures 3e and 3f). During these Δt intervals, the 35 and 0 dBZ echo heights rise on the order of 100 m per 15 s to 10.8 and 13.8 km, respectively, after an interval of 32 s, corresponding to an ascent rate of the 35 dBZ echo top of 3.1 m s^{-1}. A more distinct pattern in ΔZ on the order of ±5 dB is clear by Δt_{48} and Δt_{64}, with positive changes to reflectivity above 8 km in the core, and some negative reflectivity changes at farther distances (Figures 3g–3j). At much longer time intervals (Δt_{115} and Δt_{147}), which are the next available RHIs along this azimuth, the initial patterns of positive and negative ΔZ the same, with larger magnitudes reaching +20 dBZ primarily in the upper levels of the storm, and −10 to −15 dBZ in the mid-level storm core and downrange of the convective core (Figures 3k–3m). By the final time Δt_{147}, the 35 dBZ echo height lowered to 10.1 km, but the 0 dBZ echo top height reached 15.2 km (Figures 3m and 3n).

In contrast to the more intense cell analyzed in Case 1, this case of relatively weak convection generally had a reflectivity change less than 5 dB over a Δt of 32 s, while more distinct regions of growth and decay became obvious by Δt_{48} with $\Delta Z > 5$ dB. In both cases, growth of the convective core to higher altitudes was revealed through positive changes in reflectivity, with ascent rates of the 35 dBZ echo top height on the order of 10 m s^{-1} in the intense Case 1 and 3.1 m s^{-1} in the weaker Case 2. These two high temporal resolution examples demonstrate that weak and intense convection exhibit reflectivity changes of ~5 dB on time scales of 30 s or less, that growing parts of the storm (inferred from rising 35 dBZ echo heights) are associated with positive changes to reflectivity in the mid- to upper-levels, and that the observed largest changes on these time scales are in the upper portions of the storm where large regions of mass flux are expected as the updraft lofts water and ice higher in the atmosphere.

3.3. Case 3: The Effect of Spatial Resolution on Assessing Convective Storm Evolution

The previous two cases highlighted that changes in reflectivity at high spatial resolution (100 m) were notable even at time scales of 30 s or less. However, the ΔZ was estimated at high spatiotemporal resolution. The INCUS radar constellation is expected to have Δt values like those provided by the surface-based C-band radars, however the spatial resolution of the INCUS radars is much coarser. Here, we investigate the impact of the INCUS radar footprint (~3 km) using an example from CSAPR2 at 23:12:07 UTC on 22 June 2022 (Case 3, Figure 4). Case 3 features two convective cores, one with a 35 dBZ echo top height around 6.5 km, and a second, narrow convective core, 3 km wide, with 35 dBZ extending to 10 km (Figures 4a, 4d,

and 4g). The original, high-resolution observations are horizontally smoothed using the 3 km long boxcar filter to represent the INCUS antenna weighting function and vertically using a 0.25 km boxcar filter. The smoothed radar reflectivity field is provided in two along track resolutions at 1.5 and 3.0 km (Figures 4b, 4e, and 4h and Figures 4c, 4f, and 3i, respectively) with vertical resolution of 125 and 250 m, respectively. The 1.5 km along track (125 m vertical) integration represents a factor of 2 oversampling (Nyquist sampling, Sy et al., 2022) of the INCUS radar footprint, as selected by the INCUS mission. The 3.0 km along track (250 m vertical) resolution is shown here for comparison. Longer integration length along track is desirable for increasing the radar sensitivity, however, it comes at the expense of smearing important convective cell features (Kollias, Battaglia, et al., 2022). Overall, both the 1.5 km oversampled satellite (Figures 4b, 4e, and 4h) footprint and the 3.0 km resolution (Figures 4c, 4f, and 3i) capture the general characteristics of these cores. In looking at the changes over Δt_{94},
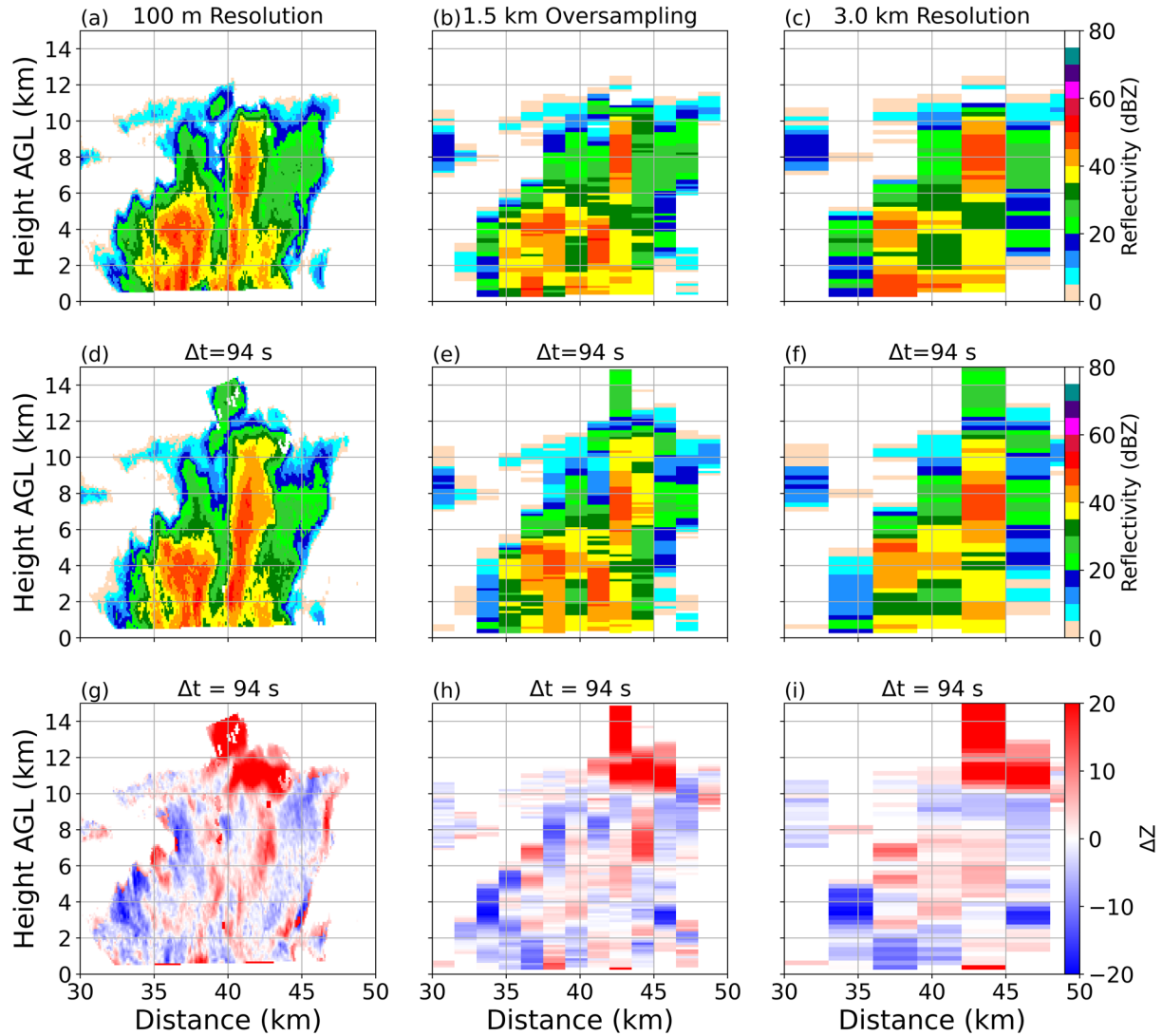
Figure 4. CSAPR2 RHIs from 22 June 2022 at 23:12:07 UTC along the azimuth of 333.1° (top row) and 94 s later (middle row) and the difference in reflectivity (bottom row) at 100 m resolution (left column), 1.5 km oversampling and 125 m vertical resolution (middle column) and 3.0 km horizontal and 250 m vertical resolution (right column).

all resolutions show large increases in reflectivity (>20 dBZ) from 10 to 12 km as the convective core at 43 km range grows. Similarly, positive ΔZ values are evident in the mid-levels (6–9 km ASL), with a stronger column of positive changes in reflectivity >~10 dB notable in the 100 m resolution with the width of ~150 m, which is also evident in the 1.5 km oversampled satellite footprint. However, this same column of positive change is missed by the 3.0 km resolution observations. This suggests that 3.0 km may be too coarse to resolve changes to convection on small spatial scales even over longer temporal intervals. Finally, all resolutions indicate that the shallower convective core at 38 km away from the radar is decaying, with large negative ΔZ or small changes to the reflectivity in the core (<±5 dB).

4. Discussion

The implementation of the MAAS framework in the recently conducted TRACER and ESCAPE field campaigns around Houston TX, allowed us to collect high spatiotemporal resolution observations in isolated convective

cells, using traditional large-reflector radars. These observations are ideal for a first evaluation of the NASA INCUS novel Δt measurement concept using real observations.

The analysis of three isolated convective cells indicated that reflectivity differences on the order of ~5 dB are observed over time scales of 20 s, underpinning the convective dynamics driving the movement of water and air in the atmosphere. Changes of up to ~20 dB were evident at longer timescales of more than 1 min in all three cases. This finding suggests that the INCUS mission selected Δt intervals are appropriate for capturing small and large ΔZ signals. For example, Case 2, an example of weaker convection illustrated changes of 10 dB were achieved within 60 s and changes larger than 20 dB at time intervals longer than 90 s. Ascent rates of the 35 dBZ reflectivity contour were 10 m s^{-1} in a rapidly growing convective core (Case 1), and were ~3 m s^{-1} in weaker isolated convection (Case 2). These results characterize the relationship between changes in reflectivity and the underlying updraft which is moving water and air upward in the atmosphere. The resulting ΔZ field contains coherent structures, a plausible indicator of large coherent convective scale updrafts being the possible mechanism for their presence.

In addition, the observations verify that the INCUS radar footprint (~3 km) is not expected to have a significant impact on determining the CMF and that the overall structure of convective cells as depicted by the radar reflectivity is well computed. This is particularly true when we oversampled by a factor of 2 the INCUS radar footprint, which will be done in the INCUS mission. In a nutshell, the INCUS radar sampling strategy is appropriate for temporal and spatial sampling of convective cores. This said, some convective elements that were smaller than the spatial resolution being considered were not resolved, even over longer time scales of 94 s. Herein we have not directly related the observed changes in reflectivity to the updraft strength from independent measurements of vertical velocity (such as from multi-Doppler techniques). A separate manuscript that focuses on a more detailed verification of the relationship between the observed ΔZ and the vertical air motion is forthcoming.

This study presents the first steps in demonstrating vertical evolution of convection using the time-resolved reflectivity, or "Δt," technique that will be utilized by the NASA INCUS mission to retrieve mass flux across the tropics. This proof-of-concept analysis has several uncertainties. First, we have assumed the contributions from horizontal advection to changes in reflectivity over short time scales are small compared to the changes due to the vertical mass flux. We are exploring machine learning techniques to mitigate the effects of horizontal advection which we can evaluate quantitatively using the 3D reflectivity data available during TRACER and ESCAPE campaigns. Second, herein we use ground-based C-band data, but the INCUS mission will rely on Ka-band from space. Impacts from the growth of precipitation sized particles, radar wavelength, microphysics, and horizontal advection are interrelated and cannot be untangled using radar data alone. High-resolution model simulations run through an INCUS instrument simulator, or forward model, will be interrogated to address these complex processes. These aspects are being analyzed quantitatively and will be presented in a forthcoming manuscript.

The results presented here demonstrate the utility of using time differencing to understand the scales of convective dynamics, both temporally and spatially. The findings will help guide future studies of convective dynamics, and our understanding of how best to utilize new and advancing observational platforms with the ability to collect data at high temporal and spatial resolutions. Future work is needed to examine if high resolution cloud resolving models can accurately capture the storm dynamical processes observed using these types of rapidly scanned data.

Data Availability Statement

The CSAPR2 radar data are available through the DOE ARM archive (Oue et al., 2023) and the CHIVO radar data are available at the National Center for Atmospheric Research Earth Observations Laboratory ESCAPE data archive (https://www.eol.ucar.edu/field_projects/escape). Gridding was done with Radx2Grid through LROSE (Bell et al., 2022). Figure 2 and some processing utilized the DOE-PyART software (Helmus & Collis, 2016). Processing code including Radx parameter files and plotting code is available from Dolan (2023).

References

Bell, M. M., Dixon, M., Lee, W.-C., Javornik, B., DeHart, J., Cha, T.-Y., & DesRosiers, A. (2022). nsf-lrose/lrose-topaz: Lrose-topaz stable final release 20220222 (lrose-topaz-2022022) [Software]. Zenodo. https://doi.org/10.5281/zenodo.6909479

Bluestein, H. B., French, M. M., PopStefanija, I., Bluth, R. T., & Knorr, J. B. (2010). A mobile phased-array Doppler radar for the study of severe convective storms. *Bulletin of the American Meteorological Society*, *91*(5), 579–600. https://doi.org/10.1175/2009BAMS2914.1

Crum, T. D., Saffle, R. E., & Wilson, J. W. (1998). An update on the NEXRAD program and future WSR-88D support to operations. *Weather and Forecasting*, *13*(2), 253–262. https://doi.org/10.1175/1520-0434(1998)013<0253:auotnp>2.0.co;2

Dolan, B. (2023). GRL_dZdT [Software]. Zenodo. https://doi.org/10.5281/zenodo.8412004

Fridlind, A. M., Li, X., Wu, D., van Lier-Walqui, M., Ackerman, A. S., Tao, W.-K., et al. (2017). Derivation of aerosol profiles for MC3E convection studies and use in simulations of the 20 May squall line case. *Atmospheric Chemistry and Physics*, *17*(9), 5947–5972. https://doi.org/10.5194/acp-17-5947-2017

Griffith, P., Gunshor, M. M., Daniels, J. M., Goodman, S. J., & Lebair, W. J. (2017). A closer look at the ABI on the GOES-R series. *Bulletin of the American Meteorological Society*, *98*(4), 681–698. https://doi.org/10.1175/bams-d-15-00230.1

Hartmann, D. L., Hendon, H. H., & Houze, R. A., Jr. (1984). Some implications of the mesoscale circulations in cloud clusters for large-scale dynamics and climate. *Journal of the Atmospheric Sciences*, *41*(1), 113–121. https://doi.org/10.1175/1520-0469(1984)041<0113:siotmc>2.0.co;2

Helmus, J. J., & Collis, S. M. (2016). The Python ARM radar toolkit (Py-ART), a library for working with weather radar data in the Python programming language [Software]. Journal of Open Research Software, *4*(1). e25. https://doi.org/10.5334/jors.119

Illingworth, A. J., Barker, H. W., Beljaars, A., Ceccaldi, M., Chepfer, H., Clerbaux, N., et al. (2015). The EarthCARE satellite: The next step forward in global measurements of clouds, aerosols, precipitation, and radiation. *Bulletin of the American Meteorological Society*, *96*(8), 1311–1332. https://doi.org/10.1175/bams-d-12-00227.1

Jensen, M., Flynn, J. H., Judd, L. M., Kollias, P., Kuang, C., Mcfarquhar, G., et al. (2022). A succession of cloud, precipitation, aerosol and air quality field experiments in the coastal urban environment. *Bulletin of the American Meteorological Society*, *103*(2), 103–105. https://doi.org/10.1175/BAMS-D-21-0104.1

Kollias, P., Battaglia, A., Lamer, K., Teserras, B. P., & Braun, S. A. (2022). Mind the gap – Part 3. Doppler velocity measurements from space. *Frontiers in Remote Sensing*, *3*, 860284. https://doi.org/10.3389/frsen.2022.860284

Kollias, P., Bharadwaj, N., Clothiaux, E., Lamer, K., Oue, M., Hardin, J., et al. (2020). The ARM radar network: At the leading edge of cloud and precipitation observations. *Bulletin of the American Meteorological Society*, *101*(5), E588–E607. https://doi.org/10.1175/bams-d-18-0288.1

Kollias, P., Palmer, R., Bodine, D., Adachi, T., Bluestein, H., Cho, J. Y., et al. (2022). Science applications of phased array radars. *Bulletin of the American Meteorological Society*, *103*(10), E2370–E2390. https://doi.org/10.1175/BAMS-D-21-0173.1

Lamer, K., Kollias, P., Luke, E. P., Treserras, B. P., Oue, M., & Dolan, B. (2023). Multisensor agile adaptive sampling (MAAS): A methodology to collect radar observations of convective cell life cycle. *Journal of Atmospheric and Oceanic Technology*. https://doi.org/10.1175/JTECH-D-23-0043.1

Marinescu, P. J., Kennedy, P. C., Bell, M. M., Drager, A. J., Grant, L. D., Freeman, S. W., & van den Heever, S. C. (2020). Updraft vertical velocity observations and uncertainties in high plains supercells using radiosondes and radars. *Monthly Weather Review*, *148*(11), 4435–4452. https://doi.org/10.1175/MWR-D-20-0071.1

Oue, M., Kollias, P., Shapiro, A., Tatarevic, A., & Matsui, T. (2019). Investigation of observational error sources in multi-Doppler-radar three-dimensional variational vertical air motion retrievals. *Atmospheric Measurement Techniques*, *12*(3), 1999–2018. https://doi.org/10.5194/amt-12-1999-2019

Oue, M., Saleeby, S. M., Marinescu, P. J., Kollias, P., & van den Heever, S. C. (2022). Optimizing radar scan strategies for tracking isolated deep convection using observing system simulation experiments. *Atmospheric Measurement Techniques*, *15*(16), 4931–4950. https://doi.org/10.5194/amt-15-4931-2022

Oue, M., Treserras, B. P., Luke, E., & Kollias, P. (2023). CSAPR2 cell-tracking data collected during TRACER [Dataset]. Web. https://doi.org/10.5439/1969992

Palmer, R., Bodine, D., Kollias, P., Schvartzman, D., Zrnić, D., Kirstetter, P., et al. (2022). A primer on phased array radar technology for the atmospheric sciences. *Bulletin of the American Meteorological Society*, *103*(10), E2205–E2230. https://doi.org/10.1175/BAMS-D-21-0172.1

Peral, E., Tanelli, S., Statham, S., Joshi, S., Imken, T., Price, D., et al. (2019). RainCube: The first ever radar measurements from a CubeSat in space. *Journal of Applied Remote Sensing*, *13*(3), 032504. https://doi.org/10.1117/1.JRS.13.032504

Sherwood, S. C., Bony, S., & Dufresne, J.-L. (2014). Spread in model climate sensitivity traced to atmospheric convective mixing. *Nature*, *505*(7481), 37–42. https://doi.org/10.1038/nature12829

Stephens, G., Freeman, A., Richard, E., Pilewskie, P., Larkin, P., Chew, C., et al. (2020). The emerging technological revolution in Earth observations. *Bulletin of the American Meteorological Society*, *101*(3), E274–E285. https://doi.org/10.1175/bams-d-19-0146.1

Stephens, G., van den Heever, S. C., Haddad, Z. S., Posselt, D. J., Storer, R. L., Grant, L. D., et al. (2020). A distributed small satellite approach for measuring convective transports in the Earth's atmosphere. *IEEE Transactions on Geoscience and Remote Sensing*, *58*(1), 4–13. https://doi.org/10.1109/TGRS.2019.2918090

Su, H., Jiang, J. H., Zhai, C., Shen, T. J., Neelin, J. D., Stephens, G. L., & Yung, Y. L. (2014). Weakening and strengthening structures in the Hadley circulation change under global warming and implications for cloud response and climate sensitivity. *Journal of Geophysical Research: Atmospheres*, *119*(10), 5787–5805. https://doi.org/10.1002/2014jd021642

Sy, O. O., Tanelli, S., Durden, S. L., Peral, E., Sacco, G. F., Chahat, N. E., et al. (2022). Scientific products from the first radar in a CubeSat (RainCube): Deconvolution, cross-validation, and retrievals. *IEEE Transactions on Geoscience and Remote Sensing*, *60*, 1–20. https://doi.org/10.1109/TGRS.2021.3073990

Tanamachi, R. L., & Heinselman, P. L. (2016). Rapid-scan, polarimetric observations of central Oklahoma severe storms on 31 May 2013. *Weather and Forecasting*, *31*(1), 19–42. https://doi.org/10.1175/WAF-D-15-0111.1

van den Heever, S. (2021). *NASA selects new mission to study storms, impacts on climate models*. NASA Earth. Retrieved from https://www.nasa.gov/press-release/nasa-selects-new-mission-to-study-storms-impacts-on-climate-models

Wehr, T., Kubota, T., Tzeremes, G., Wallace, K., Nakatsuka, H., Ohno, Y., et al. (2023). *The EarthCARE mission–science and system overview* (pp. 1–47). EGUsphere.